IOPscience iopscience.iop.org

Home Search Collections Journals About Contact us My IOPscience

A phenomenological approach to the anisotropic magnetoresistance and planar Hall effect in tetragonal $La_{2/3}Ca_{1/3}MnO_3$ thin films

This article has been downloaded from IOPscience. Please scroll down to see the full text article.

2010 J. Phys.: Condens. Matter 22 146006

(http://iopscience.iop.org/0953-8984/22/14/146006)

View the table of contents for this issue, or go to the journal homepage for more

Download details:
IP Address: 129.252.86.83
The article was downloaded on 30/05/2010 at 07:44

Please note that terms and conditions apply.

J. Phys.: Condens. Matter **22** (2010) 146006 (9pp) doi:10.1088/0953-8984/22/14/146006

A phenomenological approach to the anisotropic magnetoresistance and planar Hall effect in tetragonal $La_{2/3}Ca_{1/3}MnO_3$ thin films

J Li, S L Li, Z W Wu, S Li, H F Chu, J Wang, Y Zhang, H Y Tian and D N Zheng

National Laboratory for Superconductivity, Beijing National Laboratory for Condensed Matter Physics and Institute of Physics, Chinese Academy of Sciences, Beijing 100190, People's Republic of China

E-mail: lijie@ssc.iphy.ac.cn and dzheng@ssc.iphy.ac.cn

Received 4 December 2009, in final form 22 February 2010
Published 23 March 2010
Online at stacks.iop.org/JPhysCM/22/146006

Abstract

A $La_{2/3}Ca_{1/3}MnO_3$ Hall bar with its long dimension roughly along the hard axis [110] was fabricated on a single-crystal-like tensilely strained film on $SrTiO_3(001)$. The anisotropic magnetoresistance (AMR) and planar Hall effect (PHE) have been studied at various external magnetic fields and temperatures. A phenomenological model in the high field limit is developed, and the galvanomagnetic tensor based on a tetragonal symmetry $4/mmm$ (D_{4h}), applicable to epitaxial films on a substrate, has been obtained by expanding the tensor to the sixth order. The derived in-plane transverse resistance R_{xy} shows a $\sin 2\phi_M$ angular dependence, while the longitudinal R_{xx} is constituted by not only a two-fold $\cos 2\phi_M$ term, but also a four-fold $\cos 4\phi_M$ term due to the square symmetry of the lattice. The model is in good agreement with the experimental results in high fields, while deviations are observed near the $\langle 100 \rangle$ easy axis with the decreasing field. Close inspection of the fitting parameters reveals the evolution of these term weights with temperature and magnetic field, which is distinct from conventional ferromagnetic metals and cannot be explained by the phenomenological model. An alternative mechanism for AMR, stemming from the magnetization-induced local orbit deformation through spin–orbit interaction, as previously proposed by O'Donnell *et al*, may be prevalent in manganites and other systems of complicated crystal structure.

(Some figures in this article are in colour only in the electronic version)

1. Introduction

The planar Hall effect (PHE) was intensively studied during the mid-60s of the last century, mainly in traditional polycrystalline ferromagnetic metals and alloys [1–3], and has long been recognized as an efficient tool to probe and track magnetic anisotropy and magnetization reversal in tiny or film samples. It was widely accepted that PHE originates from the change in the scattering rate due to spin–orbit interaction, occurring when the magnetization direction is tuned with respect to the electrical current, similar to anisotropic magnetoresistance (AMR) [4, 5]. In recent years renascent interests in this effect have developed since the discovery of the so-called *giant* PHE in the diluted magnetic semiconductor (Ga, Mn)As, where a pseudo-Hall signal 10^4 times larger than that of conventional ferromagnetic metals was observed [6, 7]. Through a two-step rotation of the sample magnetization [8], the magnetic reversal by a weak in-plane sweeping magnetic field leads to two abrupt PHE voltage jumps, analogous to the giant magnetoresistance (GMR) in metallic multilayers [9]. Advanced magnetic sensors and memory components based on PHE are now expected.

Similarly, one can expect a giant PHE in manganites, where a strong spin–orbit coupling also exists. Actually,

 © 2010 IOP Publishing Ltd Printed in the UK & the USA

transverse resistivity jumps comparable in magnitude to that of (Ga, Mn)As were observed shortly after in $La_{1-x}Sr_xMnO_3$ [10, 11], and the phenomenon persists up to temperatures even higher than Curie temperature T_C. However, so far only a few studies on PHE in manganites are reported, although it is of value not only for practical devices, but also for a comprehensive understanding of spin–orbit physics itself. The latter is extremely interesting since the material shares a perovskite-like structure with many other transition-metal-based functional oxides.

On the other hand, in terms of the single domain model for homogeneous polycrystalline samples with the magnetization strictly lying in the easy plane [1, 2, 4, 5], the in-plane longitudinal (AMR) and transverse (PHE) resistivity can be described respectively as

$$\rho_{xx} = \rho_\perp + (\rho_\parallel - \rho_\perp)\cos^2\phi_M, \qquad \rho_{xy} = \tfrac{1}{2}(\rho_\parallel - \rho_\perp)\sin 2\phi_M \tag{1}$$

where ϕ_M denotes the angle between the in-plane rotating magnetization **M** and the current **J**. $\rho_\parallel$ ($\rho_\perp$) is the resistivity measured with **M** parallel (perpendicular) to **J**. When the applied external field is strong enough to saturate the sample, **M** rotates coherently according to the Stoner–Wohlfarth model, and ϕ_M equals the angle between **J** and the magnetic field **H**. Below saturation, **M** drops behind **H** and individual domains are each magnetized to their respective nearest easy axes.

In fact, equations (1) were derived phenomenologically from the cubic $m3m$ symmetry, and the magnetocrystalline anisotropy has been averaged out by integrating the randomly oriented grains, therefore it is applied only to polycrystalline samples [4]. Nevertheless, the equation has been widely used to describe AMR and PHE in epitaxial thin films [6, 12, 13], including manganites [11, 14–17]. Actually, qualitative and quantitative deviations have been observed previously in manganites [18–20], and more recently in Fe_3Si, (Ga, Mn)As and Fe_3O_4 thin films [21–23]. A four-fold oscillation of comparable magnitude has been observed superimposed on the two-fold, especially in the longitudinal resistivity, which is gradually recognized as originating from higher rank resistivity tensors [20–23]. In our present study on PHE in a single-crystal-like tensilely strained $La_{2/3}Ca_{1/3}MnO_3$ thin film grown on $SrTiO_3$(001), the longitude resistivity does not follow equation (1), even in fields higher than the saturation magnetic field. We then did a phenomenological deduction of the galvanomagnetic tensor based on a more complicated tetragonal symmetry $4/mmm$ (D_{4h}), applicable to films on a substrate, by expanding the tensor to the sixth order following Birss's scheme [24]. The derived nonzero components of higher rank tensors, as listed in the tables in the appendix, are not only appropriate for electrical resistivity, but also for other property tensors such as the thermal conductivity, the Seebeck effect and the Peltier effect [25]. The AMR and PHE expression derived can fit the experimental data in high fields well. Close inspection of the fitting coefficient may reveal the evolution of the effects with temperature and magnetic field, which can also provide useful information for microscopic theory to obtain parameters of Fermi surface model [26], thus deepening our understanding of the electronic structure in manganites.

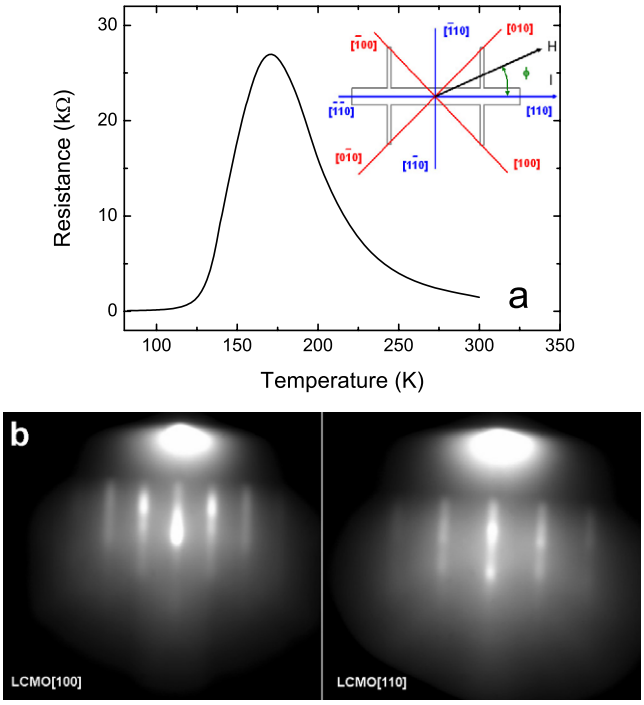

Figure 1. (a) The R–T curve of the LCMO film. The inset is the schematic diagram of the experimental configuration. The bar is roughly along LCMO[110]. (b) *In situ* RHEED monitoring of a LCMO film grown in 26 Pa oxygen, with the zone axis along (100) and (110), respectively.

2. Experimental details

The $La_{2/3}Ca_{1/3}MnO_3$ (LCMO) thin film was grown on a $SrTiO_3$(001) (STO) substrate by the pulsed laser deposition (PLD) technique from a stoichiometric ceramic target. Details of film preparation have been described elsewhere [27, 28]. The whole film growth procedure can be routinely monitored *in situ* by a high-pressure reflection high energy electron diffraction (RHEED) system, as seen in figure 1(b). The film in this study has been confirmed to be *c*-axis oriented single phase with an in-plane epitaxial relationship LCMO[100] (Mn–O bond directions) ∥ STO[100] (cube-on-cube growth). The thickness of the film is ∼1500 Å, estimated using atomic force microscopy (AFM). The temperature dependence of the film resistance was measured using the four-probe method. The insulator-to-metal transition point T_P was around 170 K, as shown in figure 1(a), lower than the bulk value. This can be attributed to the tensile strain from the film–substrate lattice mismatch, which combined with the shape anisotropy results in an easy plane parallel to the film surface [27].

The film was patterned by ultraviolet photolithography plus ion milling. The Hall bar is 100 μm in width, the separation between the voltage electrodes is 600 μm, and the long dimension of the Hall bar was aligned roughly along the LCMO[110] direction, as schematically shown in the inset of figure 1(a). The electrical contacts were coated with gold by magnetron sputtering and soldered to copper leads with indium. The sample was stuck on a specially designed copper stage and then mounted on a sample holder, so that

the sample could be rotated continuously in the film plane during measurement. The relative angle ϕ_H between **J** and **H** can be tuned from 90° to 450° and then backwards. It has been revealed that the in-plane magnetic easy axes in LCMO films on STO are along [100] and its equivalents [29]. The configuration therefore means that **J** was collinear with a hard axis of the magnetocrystalline anisotropy in LCMO. When the film behaves like a macroscopic single domain above magnetization saturation, $\phi_M = \phi_H$, otherwise, there exists a difference between ϕ_M and ϕ_H.

The magnetic fields for PHE and AMR measurements were generated by a Quantum Design Physical Property Measurement System (PPMS). Standard four-probe low frequency *ac* measurements using a lock-in voltmeter are performed with a current 10 μA at 14 Hz. The longitudinal and transverse voltages were recorded simultaneously at four different temperatures of 5, 50, 100, and 140 K and in various magnetic fields of 500, 1000, 4000, 8000, and 16 000 Oe.

3. Phenomenological model

In general, for ferromagnetic and ferrimagnetic crystals, the effect of time inversion on dynamic transport property tensors cannot be ignored, since the current **J** is time antisymmetric. Assuming that the time-inversion operation reverses the direction of spin in magnetic single crystals [24], in order to describe spin distributions the 122 Shubnikov point groups must be derived from the original 32 classical crystallographic point groups, and in the presence of a magnetic field the relationship between **E** and **J** can be nonlinear

$$E_i = \rho_{ij} J_j + R_{ijk} H_k + \cdots \tag{2}$$

where ρ_{ij} and R_{ijk} are components of the zero-field resistivity tensor and the Hall coefficient tensor, respectively.

However, when the external magnetic field is high enough to saturate the magnetization, the spin distribution in a crystal is completely determined by the field direction. This means the time symmetry of the crystal is effectively suppressed and the geometrical description of classical crystallography regains its validity. Since the crystal is magnetically saturated, the resistivity tensor is independent of the magnitude of **H**, though the direction of **H** must be taken into account. In this case, the relationship between **E** and **J** is still linear, $E_i = \rho_{ij} J_j$, where the Einstein summation convention is understood, and i and j can be in any of the three orthogonal directions. The resistivity tensor ρ_{ij} depends on the direction cosines, α_i, of the field vector, and may be expressed as series expansions in ascending powers of α_i

$$\rho_{ij}(\alpha) = a_{ij} + a_{kij}\alpha_k + a_{klij}\alpha_k\alpha_l + a_{klmij}\alpha_k\alpha_l\alpha_m + a_{klmnij}\alpha_k\alpha_l\alpha_m\alpha_n + \cdots. \tag{3}$$

Components of these high rank tensors can be dictated by the requirements of the spatial symmetry of the particular crystal, according to the Neumann principle.

Since E_i and J_j are components of a polar i-vector and a polar c-vector respectively [24], the resistivity tensors of even rank are polar c-tensors while those of odd rank are axial i-tensors. Since the phenomenon under consideration now is the dynamic transport property tensor, terms of odd orders may not be discarded. The second rank tensor $\rho_{ij}(\alpha)$ can be divided into its symmetrical and antisymmetrical parts,

$$\rho^s_{ij} = \tfrac{1}{2}[\rho_{ij}(\alpha) + \rho_{ji}(\alpha)], \qquad \rho^a_{ij} = \tfrac{1}{2}[\rho_{ij}(\alpha) - \rho_{ji}(\alpha)]. \tag{4}$$

Taking into account the Onsager reciprocity relation $\rho_{ij}(\alpha) = \rho_{ji}(-\alpha)$, ρ^s_{ij} must be an even function of α_i, and ρ^a_{ij} an odd function. Thus,

$$\rho^s_{ij}(\alpha) = a_{ij} + a_{klij}\alpha_k\alpha_l + a_{klmnij}\alpha_k\alpha_l\alpha_m\alpha_n + \cdots, \qquad \rho^a_{ij}(\alpha) = a_{kij}\alpha_k + a_{klmij}\alpha_k\alpha_l\alpha_m + \cdots \tag{5}$$

which is the generalized magnetoresistance and the generalized Hall coefficient, respectively.

It is known that the LCMO single crystal is orthorhombic of crystal class *mmm*, as expressed by the Hermann–Mauguin symbol (equivalent Schöenflies symbol D^{16}_{2h}). Grown on $SrTiO_3(001)$, due to the biaxial tensile strain from the substrate it becomes tetragonal of symmetry $4/mmm$ (D_{4h}) with the (001) direction out of plane. Therefore nonzero components of its high rank tensors can be derived with the generating elements $\sigma^{(1)}$, $\sigma^{(2)}$, and $\sigma^{(7)}$. Nevertheless, we would rather directly use the results of Birss [24] for the second, third, and fourth rank tensors, and that of Fieschi [30] for the fifth and sixth rank ones.

According to Birss (table 4 in [24]), for the point group $4/mmm$, there are constrictions

$$\begin{gathered} y^2 = x^2, \qquad z^2 = z^2; \\ yxz = -xyz, \qquad yzx = -xzy, \qquad zyx = -zxy; \\ y^4 = x^4, \qquad z^4 = z^4, \\ x^2y^2 = y^2x^2(3), \qquad x^2z^2 = y^2z^2(6) \end{gathered} \tag{6}$$

for the second, third and fourth tensor, respectively. Here, notations of the type $x^2z^2 = y^2z^2(6)$ denote the 6 equations which are the distinct permutations of $x^2z^2 = y^2z^2$.

Therefore, the polar c-tensor of second rank a_{ij} has two independent components, as listed in table A.1 in the appendix; whilst that of the fourth rank a_{klij} has seven independent components listed in table A.3, noting here the intrinsic symmetry must be considered, i.e., the first two indices k and l are interchangeable because the term $a_{klij}\alpha_k\alpha_l$ is symmetric for direction cosines α_k and α_l, and the last pair of indices i and j are also interchangeable since ρ^s_{ij} (even ranks) is a symmetrical tensor. Similarly, the third rank axial i-tensor a_{kij} has two independent components listed in table A.2, and here the last pair of indices are asymmetric.

Furthermore, Fieschi and Fumi [30] pointed out that groups which differ by the center of symmetry are equivalent for polar tensors of even rank and axial tensors of odd rank. In this sense, groups C_{4v}, D_{2d}, D_4, and D_{4h} are equivalent. Accordingly, the fifth and sixth rank tensor has constrictions

respectively

$$\begin{aligned} y^3xz &= -x^3yz\ (20), & z^3yx &= -z^3xy\ (10);\\ y^6 &= x^6, & z^6 &= z^6,\\ y^4x^2 &= x^4y^2\ (15), & y^4z^2 &= x^4z^2\ (15),\\ z^4y^2 &= z^4x^2\ (15), & y^2x^2z^2 &= x^2y^2z^2\ (45). \end{aligned} \tag{7}$$

Similarly, the six independent components of the fifth rank axial i-tensor a_{klmij} are derived and listed in table A.4, and the 15 independent components of the sixth rank polar c-tensor a_{klmnij} are in table A.5. Noting here the first three indices are interchangeable in the fifth rank tensor, this annihilates six more components. The last two are asymmetric. The first four indices and the last two are interchangeable in the sixth rank tensor.

For PHE study in the LCMO thin film on STO, the sample maintains an easy plane in the film surface, due to the interface mismatch strain as well as the demagnetization effect. The magnetization sweeps only in the easy plane, i.e., perpendicular to the z-axis of the tetragonal form, therefore we have $\alpha_1 = \cos\phi$, $\alpha_2 = \sin\phi$, and $\alpha_3 = 0$.

So

$$\begin{aligned} \rho_{11}(\alpha) &= C_0 + C_1\cos^2\phi + C_2\cos^4\phi,\\ \rho_{12}(\alpha) &= C_4\sin\phi\cos\phi,\\ \rho_{13}(\alpha) &= -C_6\sin\phi - C_7\sin^3\phi,\\ \rho_{21}(\alpha) &= C_4\sin\phi\cos\phi,\\ \rho_{22}(\alpha) &= C_0 + C_1\sin^2\phi + C_2\sin^4\phi,\\ \rho_{23}(\alpha) &= C_6\cos\phi + C_7\cos^3\phi,\\ \rho_{31}(\alpha) &= C_6\sin\phi + C_7\sin^3\phi,\\ \rho_{32}(\alpha) &= -C_6\cos\phi - C_7\cos^3\phi,\\ \rho_{33}(\alpha) &= C_8 + C_9\sin^2\phi\cos^2\phi \end{aligned} \tag{8}$$

where

$$C_0 = a_{11} + a_{1122} + a_{111122},$$

$$C_1 = a_{1111} - a_{1122} + 6a_{112211} - 2a_{111122},$$

$$C_2 = a_{111111} + a_{111122} - 6a_{112211},$$

$$C_4 = a_{1212} + 2a_{111212}, \qquad C_6 = a_{123} + 3a_{12223},$$

$$C_7 = a_{11123} - 3a_{12223}, \qquad C_8 = a_{33} + a_{1133} + a_{111133},$$

$$C_9 = 6a_{112233} - 2a_{111133}.$$

Now considering our experimental configuration, where the long dimension of the Hall bar (**J**) was aligned roughly along the LCMO[110] direction, the resistivity tensor must be transformed to the new coordinate system by the matrix

$$l = \begin{pmatrix} \cos\theta & \sin\theta & 0\\ -\sin\theta & \cos\theta & 0\\ 0 & 0 & 1 \end{pmatrix} = \begin{pmatrix} \frac{\sqrt{2}}{2} & \frac{\sqrt{2}}{2} & 0\\ -\frac{\sqrt{2}}{2} & \frac{\sqrt{2}}{2} & 0\\ 0 & 0 & 1 \end{pmatrix} \tag{9}$$

whose elements have been determined by the relative orientation of the old and new sets of axes. Then the longitudinal and transverse resistivities in our experimental configuration are

$$\begin{aligned} \rho_{xx} &= C_0' + C_1'\sin 2\phi + C_2'\cos 4\phi,\\ \rho_{xy} &= -C_3'\cos 2\phi \end{aligned} \tag{10}$$

respectively, where

$$\begin{aligned} C_0' &= C_0 + \tfrac{1}{2}C_1 + \tfrac{3}{8}C_2 = a_{11} + \tfrac{1}{2}(a_{1111} + a_{1122})\\ &\quad + \tfrac{3}{8}(a_{111111} + a_{111122} + 2a_{112211}),\\ C_1' &= \tfrac{1}{2}C_4 = \tfrac{1}{2}a_{1212} + a_{111212},\\ C_2' &= \tfrac{1}{8}C_2 = \tfrac{1}{8}(a_{111111} + a_{111122} - 6a_{112211}),\\ C_3' &= \tfrac{1}{2}(C_1 + C_2) = \tfrac{1}{2}(a_{1111} - a_{1122} + a_{111111} - a_{111122}). \end{aligned}$$

Note here that ϕ is the angle between magnetization **M** and the [100] direction, and $\phi = \phi_M + 45°$, where ϕ_M is the angle of **M** with respect of **J**. Then equations (10) can be expressed in ϕ_M as

$$\begin{aligned} \rho_{xx} &= C_0' + C_1'\cos 2\phi_M - C_2'\cos 4\phi_M,\\ \rho_{xy} &= C_3'\sin 2\phi_M. \end{aligned} \tag{11}$$

Clearly, the longitudinal resistivity ρ_{xx} is constituted by not only a two-fold $\cos 2\phi_M$ term, but also a four-fold $\cos 4\phi_M$ oscillation; while in the transverse case the curve is hardly changed with respect to equation (1).

4. Experimental results and discussion

The angular dependence of the longitudinal resistance R_{xx} and the transverse resistance R_{xy} measured in 8000 Oe at different temperatures 5, 50, 100, and 140 K (slightly below T_P) are shown in figure 2. For clarity, only the backward data are plotted. Here the constant part in R_{xy} has been removed, which is actually a contribution from R_{xx} due to an imperfect geometrical alignment of the transverse contacts. To fit the experimental data, equations (11) are revised as

$$\begin{aligned} R_{xx} &= C_0'' + C_1''\cos 2\phi_M + C_2''\cos 4\phi_M + C_m\sin 2\phi_M,\\ R_{xy} &= C_3''\sin 2\phi_M \end{aligned} \tag{12}$$

where an extra $\sin 2\phi$ term is added on account of the slight misalignment of the Hall bar with regard to the LCMO [110] direction. The C_m value is actually fairly small as compared with C_1'' and C_2''. The fitting curves are also given in the figure and the parameters are listed in table 1. For LCMO films on STO the coercivity and the in-plane magnetocrystalline anisotropic field are all well below 500 Oe, therefore a 8000 Oe field should be high enough to saturate the sample. That is, the magnetization in the sample is defined solely by the direction of the external magnetic field, so that the whole sample is in a *macroscopic* single domain state during the field sweeps. As a result, here the precondition of the phenomenological model dictated above is fulfilled, and thus the data can be perfectly fitted. As predicted, the longitudinal resistance R_{xx} actually consists of a $\cos 4\phi_M$ term as well as a $\cos 2\phi_M$

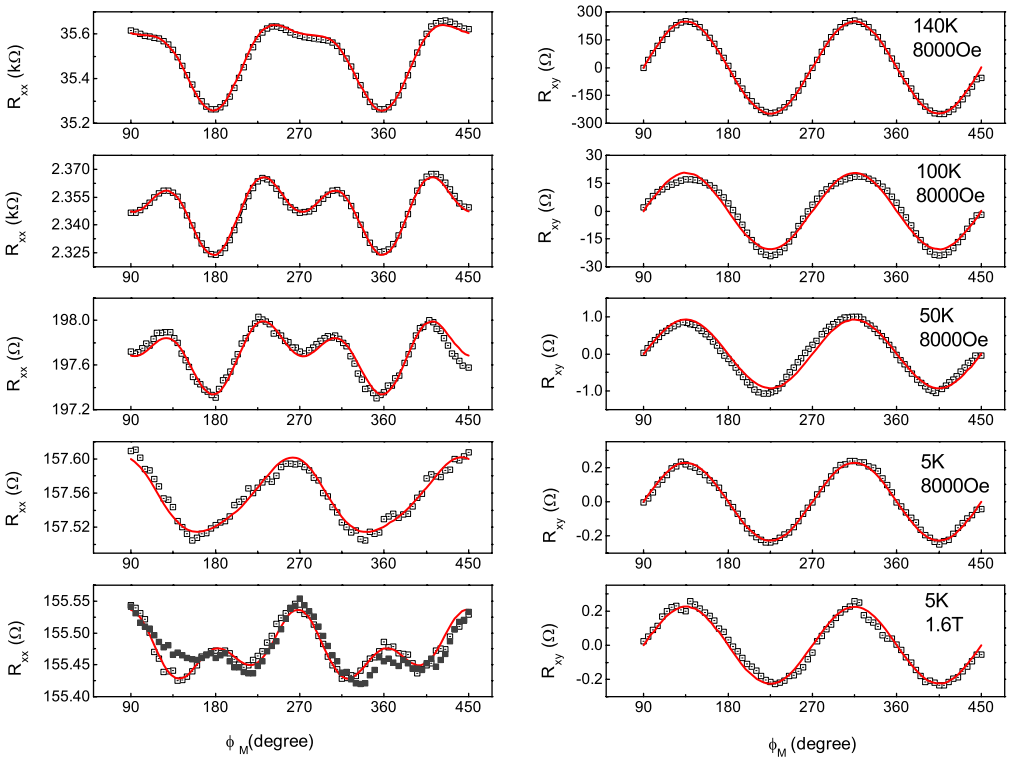

Figure 2. Angular dependence of R_{xx} and R_{xy} measured in high fields of 8000 or 16 000 Oe at different temperatures. The scattered spots are experimental data and the lines are fitting results using equations (12).

Table 1. Fitting results using equations (12). The data enclosed in brackets are of lower reliability since in low fields the phenomenological model is no longer applicable.

T (K)	H (Oe)	C_0'' (Ω)	C_1'' (Ω)	C_2'' (Ω)	C_3'' (Ω)	C_2''/C_1''
5	16 000	$155.47_{\pm 0.0009}$	$-0.031_{\pm 0.001}$	$0.032_{\pm 0.001}$	$-0.224_{\pm 0.004}$	−1.0393
5	8 000	$157.555_{\pm 0.0008}$	$-0.039_{\pm 0.001}$	$0.006_{\pm 0.001}$	$-0.22_{\pm 0.002}$	−0.1435
5	4 000	—	—	—	$-0.209_{\pm 0.004}$	—
5	1 000	—	—	—	$(-0.164_{\pm 0.008})$	—
5	500	—	—	—	$(-0.154_{\pm 0.007})$	—
50	16 000	—	—	—	$-0.68_{\pm 0.01}$	—
50	8 000	$197.705_{\pm 0.004}$	$-0.173_{\pm 0.005}$	$-0.193_{\pm 0.005}$	$-0.92_{\pm 0.01}$	1.1156
50	4 000	—	—	—	$-0.94_{\pm 0.02}$	—
50	1 000	—	—	—	$(-0.76_{\pm 0.03})$	—
50	500	—	—	—	$(-0.56_{\pm 0.03})$	—
100	8 000	$2348.2_{\pm 0.1}$	$-11.7_{\pm 0.2}$	$-12.6_{\pm 0.2}$	$-20.5_{\pm 0.4}$	1.0806
140	8 000	$35\,493_{\pm 1}$	$-173_{\pm 2}$	$-62_{\pm 2}$	$-248_{\pm 2}$	0.3593
140	1 000	$69\,190_{\pm 4}$	$-379_{\pm 6}$	$-158_{\pm 6}$	$-314_{\pm 5}$	0.4156
140	500	$(73\,230_{\pm 6})$	$(-380_{\pm 9})$	$(-92_{\pm 9})$	$(-241_{\pm 4})$	(0.2418)

term, corresponding to a biaxial anisotropy due to the in-plane square symmetry of the lattice, and a uniaxial anisotropy due to the two-fold symmetry of the current, respectively. The transverse resistance R_{xy} basically follows the $\sin 2\phi_M$ function, the same as expected for polycrystalline samples. At 5 K the data in a 16 000 Oe field are also selected to ensure the high field prerequisite, where both the forward and reverse sweeps are shown, since at low temperatures the magnetocrystalline anisotropic field is higher. Obviously, although the angular dependence of the data at 5 K is roughly a 'W' shape, especially in a 8000 Oe field, while that at other temperatures are 'M' shape, the data can all be well fitted using equations (12), except that here C_2'' is positive whereas at other temperatures it is negative.

The pseudo-Hall signal is conventionally defined as $R_{\parallel} - R_{\perp}$, the amplitude of R_{xx} or R_{xy} oscillations (equations (1)). It is usually positive in transition metal polycrystallines. To investigate the evolution of the signals with temperature for the LCMO film, in the top panel of figure 3 the fitting parameters C_1'' and C_3'', prefactors of $\cos 2\phi_M$ in R_{xx} and $\sin 2\phi_M$ in R_{xy} respectively, in varied fields are plotted versus temperature. Clearly, the two parameters are negative at all the temperatures. At 140 K in a 1000 Oe field (see table 1), the PHE signal C_3'' is quite large ~ -314 Ω. It decreases remarkably with cooling,

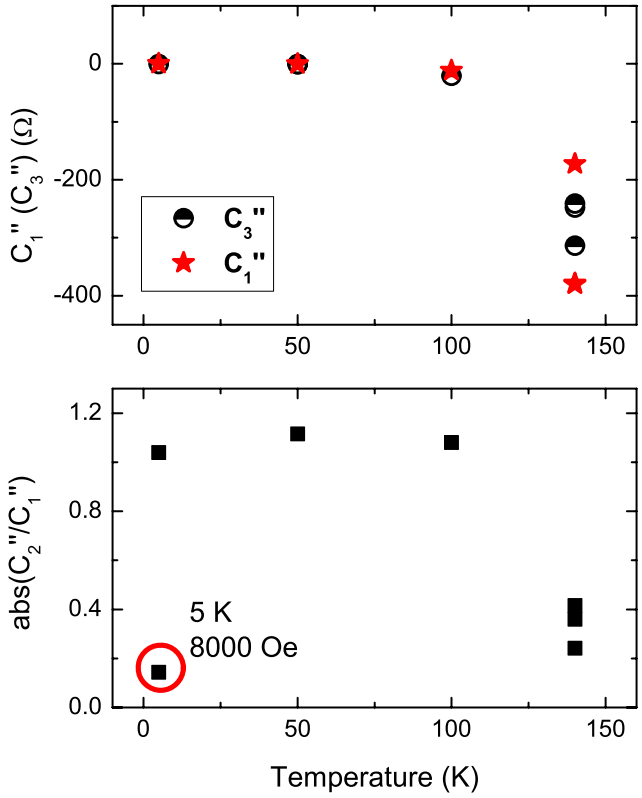

Figure 3. The temperature dependence of the fitting parameters C_1'' and C_3'' (top), and the ratio C_2''/C_1'' (bottom) of equations (12).

but only changes slightly with field, and is $\sim -20\ \Omega$ at 100 K, and is further reduced to only ~ -0.22 at 5 K. The C_1'' value roughly follows the same trend. The observation is distinct from that in ferromagnetic metals like cobalt, also having been reported previously. The decrease of AMR and PHE signals with temperature below T_C has been widely observed in crystalline samples of complicated lattice structures such as manganite [10, 14–17, 19], Fe_3O_4 [13], and Fe_3Si [21]. This is substantially different from that in conventional metals, which would behave like the square of magnetization and thus approach a saturation value at low temperatures. This appears to be in connection with the temperature dependence of the sample resistance, and thus may indicate a unique spin–orbit coupling mechanism in the complicated crystal systems.

Although the magnitude of all the three parameters decreases with cooling, in accordance with the metallic transport behavior of the sample, the relative weight of the biaxial anisotropy with respect to the uniaxial one varies with temperature. In the bottom panel of figure 3, the biaxial prefactor C_2'' is normalized with C_1''. The absolute value of C_2''/C_1'' drops rapidly with warming, meaning the relative contribution from the $\cos 4\phi_M$ term decreases with increasing temperature. Nevertheless, it is noted that the sign of C_2'' at 5 K is opposite to the others (see table 1), and in 8000 Oe the ratio is very small, as circled in red in the figure. This may be on account of a field-induced reorientation of the easy axis from ⟨100⟩ to ⟨110⟩, which so far has never been reported; or perhaps a structural change caused by the 110 K phase transition of the STO substrate. Further experiments are needed. As for the field dependence, O'Donnell *et al* [19] have claimed a decrease of the normalized AMR signal with increasing magnetic field in LCMO films on STO. Ramos *et al* [23] also argued that in Fe_3O_4 thin films the magnitude of the 'additional anisotropy' grew with increasing field and decreasing temperature. However, it seems not to be that straightforward here. We can see from table 1 that, at 140 K the ratio increases when the field is raised from 500 to 1000 Oe, but reduces when the field is further increased to 8000 Oe. Apparently further experiments at different fields are needed to clarify this issue [22].

Finally the angular dependence of R_{xx} and R_{xy} measured at 140 K in external magnetic fields 8000, 1000, and 500 Oe are shown in figure 4. Both the down- and the up-sweep

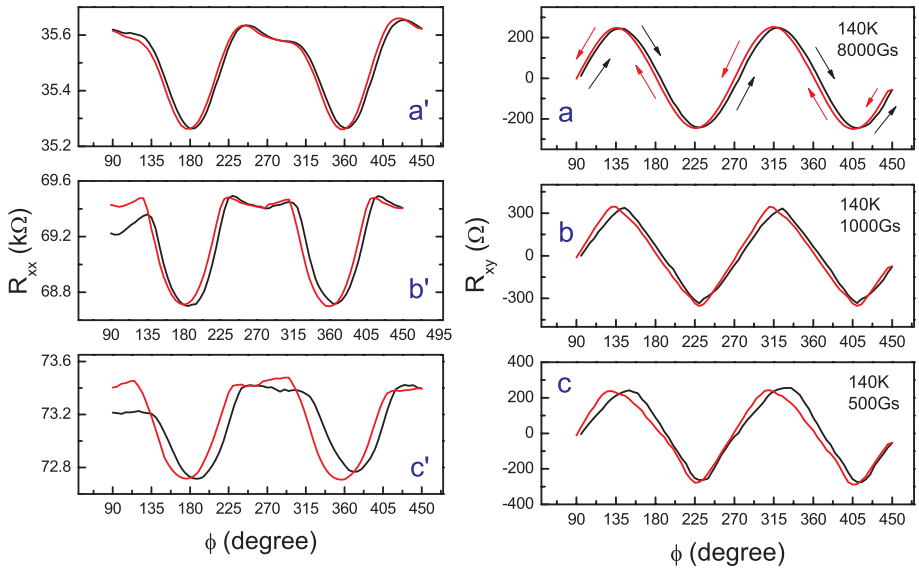

Figure 4. Angular dependence of R_{xx} and R_{xy} measured at 140 K in sweeping fields of fixed magnitude 8000, 1000, and 500 Oe respectively. The sample was rotated forwards from 90° to 450°, and then backwards.

data are plotted. It is noted that in high fields the curves almost superimpose on each other, showing only very small hysteresis. With the field decreasing, hysteresis appears in R_{xx}, especially around the in-plane easy axes LCMO⟨100⟩, say 135°, 225°, 315°, and 405(45)°. The R_{xy} data also show obvious distortions at these angles. It is noted that the resistance peaks at 135° and 315° are broadened while the valleys at 45° and 225° are deepened. In fact the phenomenon is more pronounced as the temperature and the external field are both reduced. However, no abrupt jump is observed. This means that, even in the case of 140 K, where the magnetocrystalline anisotropy energy is relatively low, in fields below 1000 Oe the film is still not in a complete single domain state. This may be due to the relatively large thickness of the film [31]. A kind of multi-domain state emerges as the sweeping magnetic field comes across the easy axes, where it is more difficult for the external field to drag the sample magnetization with it. Therefore, while at high temperatures in high magnetic fields the sample can be described using the single domain model expressed by equations (12), its magnetocrystalline anisotropy and perhaps shape anisotropy cannot be ignored at low temperatures in low fields.

We know that the most traditional explanation of AMR and PHE in ferromagnetic metals and alloys is the change in scattering rate of the charge carriers, which relates only to the angle between **M** and **J**, with no concern given to the crystal symmetry. The phenomenological model developed in this paper elucidates the effect of crystal axes and space anisotropy on AMR, which are actually a reflection of the anisotropy in the Fermi surface. However, the theory still fails in interpreting the strong temperature and field dependence of the AMR/PHE signal and the C_2''/C_1'' ratio. It has been widely observed in complicated crystal systems such as (Ga, Mn)As, Fe_3Si, Fe_3O_4, and manganite, that the AMR signal peaks around the temperature of the maximum resistance and shows a substantial field dependency. This may suggest an alternative mechanism distinct from that in traditional ferromagnets, which may share some features with the colossal magnetoresistance (CMR) effect. It is worth noting that O'Donnell *et al* [19] and Viret *et al* [32] have proposed a mechanism of field-induced Mn 3d and O 2p orbital deformation by means of spin–orbit coupling. Rotation of the magnetization continuously deforms the local electron orbitals through the spin–orbit interaction, which then changes the orbital overlap between neighboring Mn and O ions and in turn modulates the conductivity through changing the hopping probability. In order to look at in detail the origin of AMR in ferromagnetic complicated systems, more experiments are needed to determine the independent components of the galvanomagnetic tensors at different temperatures.

5. Conclusions

In summary, a phenomenological model base on a tetragonal film with D_{4h} symmetry has been successfully developed and the high rank resistivity tensors are given explicitly. A $\cos 4\phi_M$ term appears in the angular dependence of the longitudinal resistance R_{xx} in a LCMO bar along [110], which originates from the four-fold symmetry of the lattice. The experimental data can be well fitted by using the model except that the relative fraction of the $\cos 2\phi_M$ and the $\cos 4\phi_M$ terms changes with temperature and field. A qualitatively different mechanism stemming from the magnetization-induced local orbit deformation through spin–orbit interaction may be responsible for the AMR effect in manganites and other systems of complicated crystal structure.

Acknowledgments

The project was sponsored by the National Natural Science Foundation of China under grant Nos 50672125, 10974229, 10974243, and 10911130357, and the Ministry of Science and Technology (2006CB921107 and 2007AA03Z214). The authors would like to thank Professor D Wu of Nanjing University for helpful discussions and Mr S K Su for Hall measurements.

Appendix

Table A.1. The forms of the second rank tensor a_{ij} (polar c-tensor) of the symmetry class $4/mmm$, from table 4 in reference [24].

ij	11	22	33	23	32	31	13	12	21
	11	11	33						

Table A.2. The forms of the third rank tensor a_{kij} (axial i-tensor) of the symmetry class $4/mmm$, from table 4 in reference [24].

ij	11	22	33	23	32	31	13	12	21
α_1				123	−123				
α_2						123	−123		
α_3								312	−312

Table A.3. The forms of the fourth rank tensor a_{klij} (polar c-tensor) of the symmetry class $4/mmm$, from table 4 in reference [24].

ij	11	22	33	23	32	31	13	12	21
α_1^2	1111	1122	1133						
α_2^2	1122	1111	1133						
α_3^2	3311	3311	3333						
$\alpha_2\alpha_3$				2323*2	2323*2				
$\alpha_3\alpha_1$						2323*2	2323*2		
$\alpha_1\alpha_2$								1212*2	1212*2

Table A.4. The forms of the fifth rank tensor a_{klmij} (axial i-tensor) of the symmetry class $4/mmm$, from reference [30].

ij	11	22	33	23	32	31	13	12	21
α_1^3				11123	−11123				
α_2^3						11123	−11123		
α_3^3								33312	−33312
$\alpha_1\alpha_2^2$				12223*3	−12223*3				
$\alpha_2\alpha_3^2$						23331*3	−23331*3		
$\alpha_3\alpha_1^2$								11312*3	−11312*3
$\alpha_1\alpha_3^2$				23331*3	−23331*3				
$\alpha_2\alpha_1^2$						12223*3	−12223*3		
$\alpha_3\alpha_2^2$								11312*3	−11312*3
$\alpha_1\alpha_2\alpha_3$	12311*6	−12311*6							

Table A.5. The forms of the sixth rank tensor a_{klmnij} (polar c-tensor) of the symmetry class $4/mmm$, from reference [30].

ij	11	22	33	23	32	31	13	12	21
α_1^4	111111	111122	111133						
α_2^4	111122	111111	111133						
α_3^4	333311	333311	333333						
$\alpha_2^2\alpha_3^2$	223311*6	223322*6	223333*6						
$\alpha_3^2\alpha_1^2$	223322*6	223311*6	223333*6						
$\alpha_1^2\alpha_2^2$	112211*6	112211*6	112233*6						
$\alpha_1^2\alpha_2\alpha_3$				112323*12	112323*12				
$\alpha_2^2\alpha_3\alpha_1$						112323*12	112323*12		
$\alpha_3^2\alpha_1\alpha_2$								331212*12	331212*12
$\alpha_2^3\alpha_3$				111313*4	111313*4				
$\alpha_3^3\alpha_1$						333131*4	333131*4		
$\alpha_1^3\alpha_2$								111212*4	111212*4
$\alpha_3^3\alpha_2$				333131*4	333131*4				
$\alpha_1^3\alpha_3$						111313*4	111313*4		
$\alpha_2^3\alpha_1$								111212*4	111212*4

References

[1] Ky V D 1968 *Phys. Status Solidi* **26** 565

[2] Hirsch A A and Kleefeld J 1971 *IEEE Trans. Magn.* **7** 733 (presented at the 1971 InterMag Conference, Denver, Colo., April 13–16)

[3] Yau K L and Chang J T H 1971 *J. Phys. F: Met. Phys.* **1** 38

[4] McGuire T R and Potter R I 1975 *IEEE Trans. Magn.* **11** 1018

[5] Thompson D A, Romankiw L T and Mayadas A F 1975 *IEEE Trans. Magn.* **11** 1039

[6] Tang H X, Kawakami R K, Awschalom D D and Roukes M L 2003 *Phys. Rev. Lett.* **90** 107201

[7] Sarma S D 2003 *Nat. Mater.* **2** 292

[8] Cowburn R P, Gray S J, Ferré J, Bland J A C and Miltat J 1995 *J. Appl. Phys.* **78** 7210

[9] Gould C, Röster C, Jungwirth T, Girgis E, Schott G M, Giraud R, Brunner K, Schmidt G and Molenkamp L W 2004 *Phys. Rev. Lett.* **93** 117203

[10] Bason Y, Kleina L, Yau J-B, Hong X and Ahn C H 2004 *Appl. Phys. Lett.* **84** 2593

[11] Bason Y, Klein L, Yau J-B, Hong X, Hoffman J and Ahn C H 2006 *J. Appl. Phys.* **99** 08R701

[12] Bowen M, Friedland K-J, Herfort J, Schönherr H-P and Ploog K H 2005 *Phys. Rev.* B **71** 172401

[13] Fernndez-Pacheco A, De Teresa J M, Orna J, Morellon L, Algarabel P A, Pardo J A, Ibarra M R, Magen C and Snoeck E 2008 *Phys. Rev.* B **78** 212402

[14] Eckstein J N, Bozovic I, O'Donnell J, Onellion M and Rzchowski M S 1996 *Appl. Phys. Lett.* **69** 1312

[15] Amaral V S, Lourenço A A C S, Araújo J P, Pereira A M, Sousa J B, Tavares P B, Vieira J M, Alves E, da Silva M F and Soares J C 2000 *J. Appl. Phys.* **87** 5570

[16] Infante I C, Laukhin V, Sánchez F, Fontcuberta J, Melnikov O, Yu Gorbenko O and Kaul A R 2006 *J. Appl. Phys.* **99** 08C502

[17] Infante I C, Laukhin V, Sánchez F and Fontcuberta J 2006 *Mater. Sci. Eng.* B **126** 283

[18] Bibes M, Martínez B, Fontcuberta J, Trtik V, Ferrater C, Sánchez F, Varela M, Hiergeist R and Steenbeck K 2000 *J. Magn. Magn. Mater.* **211** 206

[19] O'Donnell J, Eckstein J N and Rzchowski M S 2000 *Appl. Phys. Lett.* **76** 218
[20] Bason Y, Hoffman J, Ahn C H and Klein L 2009 *Phys. Rev.* B **79** 092406
[21] Muduli P K, Friedland K-J, Herfort J, Schönherr H-P and Ploog K H 2005 *Phys. Rev.* B **72** 104430
[22] Wu D, Wei P, Johnston-Halperin E, Awschalom D D and Shi J 2008 *Phys. Rev.* B **77** 125320
[23] Ramos R, Arora S K and Shvets I V 2008 *Phys. Rev.* B **78** 214402
[24] Birss R R 1964 *Symmetry and Magnetism* (Amsterdam: North-Holland)
[25] Grimmer H 1993 *Acta Crystallogr.* A **49** 763–71
[26] Akgöz Y C and Saunders G A 1974 *J. Phys. C: Solid State Phys.* **9** 1655
[27] Li J, Wang P, Xiang J Y, Zhu X H, Peng W, Chen Y F, Zheng D N and Li Z W 2005 *Appl. Phys. Lett.* **86** 112514
[28] Li J, Wang P, Peng W, Xiang J Y, Zhu X H, Chen Y F, Wang F B and Zheng D N 2006 *Appl. Phys.* A **83** 313
[29] O'Donnell J, Rzchowski M S, Eckstein J N and Bozovic I 1998 *Appl. Phys. Lett.* **72** 1775
[30] Fieschi B and Fumi F G 1953 *Nuovo Cimento* **10** 865
[31] Shin D Y, Chung S J and Lee S 2007 *Phys. Rev. Lett.* **98** 047201
[32] Viret M, Gabureac M, Ott F, Fermon C, Barreteau C, Autes G and Guirado-Lopez R 2006 *Eur. Phys. J.* B **51** 1